A. Agarwal, H. Joshi and A. Kumar,
*S. Afr. J. Chem.*, 2011, **64**, 218–224,
<http://journals.sabinet.co.za/sajchem/>.



# Synthesis, Characterization and Application of Nano Lepidocrocite and Magnetite in the Degradation of Carbon Tetrachloride

**Ashutosh Agarwal[a,*], Himanshu Joshi[a] and Anil Kumar[b]**

[a]*Department of Hydrology, Indian Institute of Technology Roorkee, Roorkee 247667, India.*
[b]*Department of Chemistry, Indian Institute of Technology Roorkee, Roorkee 247667, India.*

Received 3 February 2011, revised 19 September 2011, accepted 4 October 2011.

ABSTRACT

**Degradation of halogenated organic compounds using nanoparticles is one of the innovative technologies in environmental remediation. In the present study, the synthesis, characterization and application of lepidocrocite (FeOOH) and magnetite ($Fe_3O_4$) nanoparticles for the remediation of water contaminated with carbon tetrachloride ($CCl_4$) has been investigated. The synthesized nanoparticles were characterized by using advanced instrumental techniques such as field emission scanning electron microscopy (FESEM) and X-ray diffraction (XRD). The synthesized FeOOH and $Fe_3O_4$ nanoparticles were found to have an average crystallite size of 10.94 nm and 18.10 nm, respectively. Batch degradation experiments for the degradation of $CCl_4$ were carried out separately using both of the above synthesized nanoparticles. The degradation reactions were found to be first-order while using $Fe_3O_4$ and second-order while using FeOOH nanoparticles. Moreover, the reactivity of freshly synthesized $Fe_3O_4$ nanoparticles was found to be much higher than that of FeOOH nanoparticles.**

KEYWORDS

**Nanoparticles, magnetite, lepidocrocite, carbon tetrachloride, degradation kinetics.**

## 1. Introduction

Chlorinated organic compounds like $CCl_4$ are widely used as extracting agents as well as synthetic intermediates for plastics and herbicides.[1] Such compounds are highly carcinogenic and mutagenic. These compounds find their way into the soil and groundwater through improper storage and spills. There is a great need to develop a cost-effective technology in order to degrade such contaminants from wastewater effectively. Chlorinated organic compounds are commonly treated by various methods like adsorption on activated carbon, bio-transformations and abiotic reductive transformations. Permeable reactive barriers coated with zero-valent iron have proved to be a prominent method for the reductive elimination of chlorinated organic compounds. Various other zero-valent metals have also been explored for reductive transformation of halogenated organic compounds.[2–10]

Many researchers have synthesized nanoscale particles for the treatment of chlorinated organic compounds.[4,11–13] Fe/Pd nanoparticles were found to be much more effective than micro-scale Fe particles in degrading chloroethenes.[12] Similarly Fe/Ni nanoparticles were found to be more effective for the dehalogenation of tetrachloroethene.[11] The use of synthesized magnetite nanoparticles has also been studied previously for the remediation of contaminated groundwater with molasses-based distillery waste.[14] A remarkable decline in the values of colour, total organic carbon, and total dissolved solids was observed upon treatment of the contaminated groundwater with freshly synthesized magnetite nanoparticles. In order to study the feasibility of using magnetite and lepidocrocite nanoparticles for the chemical degradation of carbon tetrachloride, we performed a comparative kinetic study, the results of which we report here.

* To whom correspondence should be addressed. E-mail: wheland@rediffmail.com

## 2. Material and Methods

### 2.1. Chemicals

Assay-grade anhydrous ferric chloride ($FeCl_3$) and sodium borohydride ($NaBH_4$) were obtained from Qualigens, India, and Merck, India, respectively. HPLC-grade methanol ($CH_3OH$) was also purchased from Qualigens, India. All the solutions were prepared by using double-distilled water (conductivity 1.5 $\mu$S cm$^{-1}$; pH 8.1).

### 2.2. Synthesis of Lepidocrocite (FeOOH) Nanoparticles

The synthesis of nanoscale FeOOH was carried out in a similar way as the synthesis of nano zero-valent iron by using sodium borohydride ($NaBH_4$) as the reductant.[12] A volume of 100 mL (0.25 M) of an aqueous solution of sodium borohydride ($NaBH_4$) was added dropwise with constant vigorous stirring to 100 mL (0.045 M) of ferric chloride ($FeCl_3$) aqueous solution. All the solutions were prepared in double-distilled water having an electrical conductivity of 1.5 $\mu$S cm$^{-1}$ and a pH value of 8.1. After constant vigorous stirring for about 20 minutes, a jet-black precipitate was obtained. This precipitate was separated from the solution by centrifuging the product at 1200 rpm for 10 min. The particles were then washed 3 to 4 times with 150 mL of double-distilled water. After washing they were left in the open for 24 h, which resulted in the formation of reddish brown FeOOH particles. These reddish brown particles were then dried under vacuum at 80 °C for 4 h. After drying the particles were finely ground with a pestle in an agate mortar and were stored in an airtight bottle.

### 2.3. Synthesis of Magnetite ($Fe_3O_4$) Nanoparticles

$Fe_3O_4$ nanoparticles were synthesized in a similar fashion as mentioned for FeOOH except that the washing was done 3–4

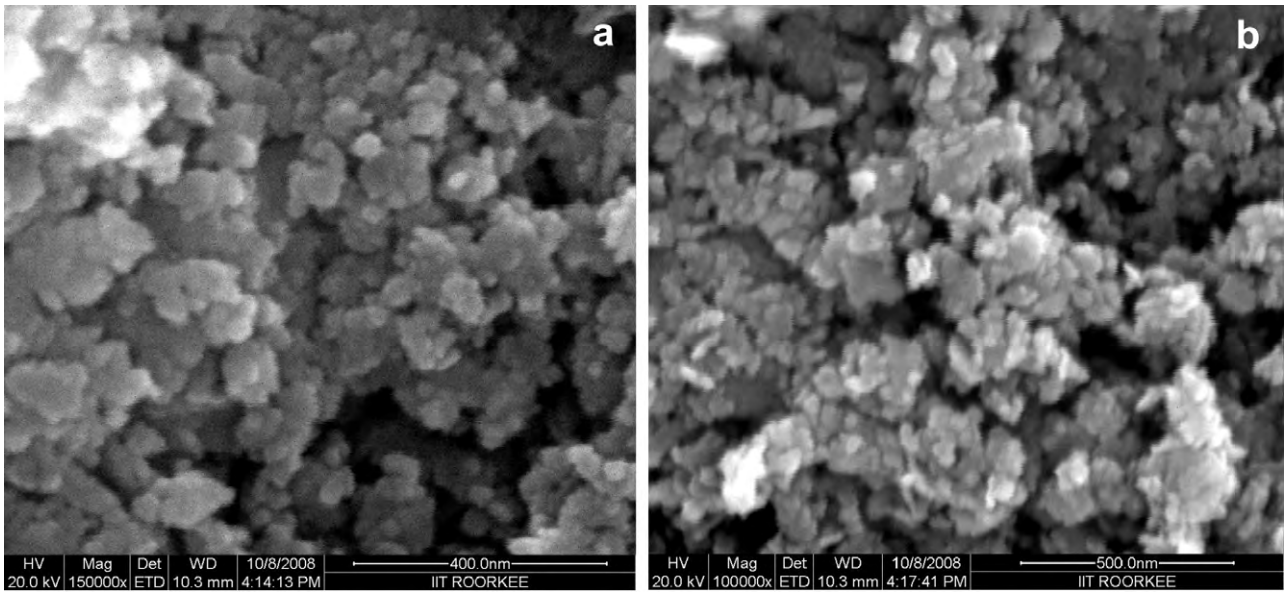


**Figure 1** FESEM images of (**a**) FeOOH and (**b**) $Fe_3O_4$ nanoparticles.

times using 150 mL of anhydrous methanol. Immediately after washing the jet-black particles were dried under vacuum at 80 °C for 4 h. Soon after drying the particles were finely ground in an agate mortar and stored in an airtight bottle.

### 2.4.Characterization of Nanoparticles

The surface morphology of the synthesized FeOOH and $Fe_3O_4$ nanoparticles was determined by making thin films of the particles over a thin transparent glass slide of 1 × 1 cm, sputter-coating with gold and observing with a field emission scanning electron microscope (FESEM, Quanta 200 FEG, FEI Netherlands) operated at 20 kV connected to an energy dispersive X-ray (EDX) analysis instrument. EDX was used to quantify the percentage Fe in the nano FeOOH and $Fe_3O_4$. A quantitative analysis was conducted by standardless analysis. A standardless analysis quantifies Fe by calculating the area under the peak of each identified element, and after accounting for the accelerating voltage of the beam to produce the spectrum, performs calculations to create sensitivity factors that convert the area under the peak into atomic percentage.

X-ray diffraction (XRD) analysis of the mineralogical characteristics of the nanoscale particles was carried out by using an XRD difractometer (Bruker AXS D8 Advance) at 30 kV and 30 mA with iron $K_\alpha$ radiation ($\lambda$ = 1.93604 Å). Particle samples were placed into a zero background holder and the scan rate of $2\theta$ was set at 0.5° per minute. The Scherrer equation[15] was used to estimate the crystallite size of the nano-scale particles from their XRD pattern:

$$t = \frac{K \times \lambda}{B \times \cos\theta_B} \quad (1)$$

where t is the average crystallite size, K is a constant (0.9), B is the full width in radians at half maximum intensity, $\lambda$ is the X-ray wavelength and $\theta_B$ is the angle at maximum diffraction curve intensity.

### 2.5. Experimental Setup

Degradation of $CCl_4$ by both FeOOH and $Fe_3O_4$ nanoparticles was studied by monitoring the chloride ion concentration at different times and by using four different $CCl_4$ starting concentrations. For these purposes four different sets of solutions having $CCl_4$ concentrations of 250 ppm, 500 ppm, 750 ppm and 1000 ppm were prepared in a mixture of 20 mL methanol and 40 mL double-distilled water at room temperature. To each of these solutions 0.22 g of the synthesized FeOOH and $Fe_3O_4$ nanoparticles were added separately in two separate batches. The mixtures thus obtained were manually stirred at regular intervals. The chloride ion concentration was measured in each of these solutions at regular intervals with an Orion expandable ion analyzer combined with an Orion chloride electrode model 9417B and Orion silver chloride reference electrode model 9002. The order and rate constant of both the degradation reactions were determined by using the differential method. The rate of the reaction may be expressed as:

$$-dC/dt = kC_i^n \quad (2)$$

On taking logarithms of the modulus values of both sides of the above equation, we get

$$\log(dC/dt) = \log k + n \log C_i \quad (3)$$

where dC/dt is the change in the concentration with time, k is the rate constant, $C_i$ is the initial concentration and n is the order of the reaction.

Two different sets of curves were then plotted for each of the FeOOH and $Fe_3O_4$-assisted degradations. These were plots of the chloride ion concentrations (ppm) against reaction time (min). In order to study the kinetics, the initial rates of reaction were determined from the slopes of the tangents to the above curves evaluated at time t = 1.5 min. For each set of curves the logarithmic values of the slope (dC/dt) of the tangents thus obtained were plotted against the logarithm of the initial $CCl_4$ concentrations ($C_i$). From Equation 3, the plot of log (dC/dt) against log $C_i$ gives a straight line, the slope of which gives the order (n) of the reaction. The y-intercept of the above plot gives the log value of the rate constant (k). Hence the orders of the reactions as well as the initial rate constants were evaluated.

## 3. Results and Discussion

### 3.1. Properties of the Nanoparticles

The FESEM images (Fig. 1a,b) of the FeOOH and $Fe_3O_4$ nanoparticles suggest that the average diameter of the nanoparticles is of the order of 15–30 nm and 20–30 nm, respectively. The EDAX plots of FeOOH and $Fe_3O_4$ nanoparticles

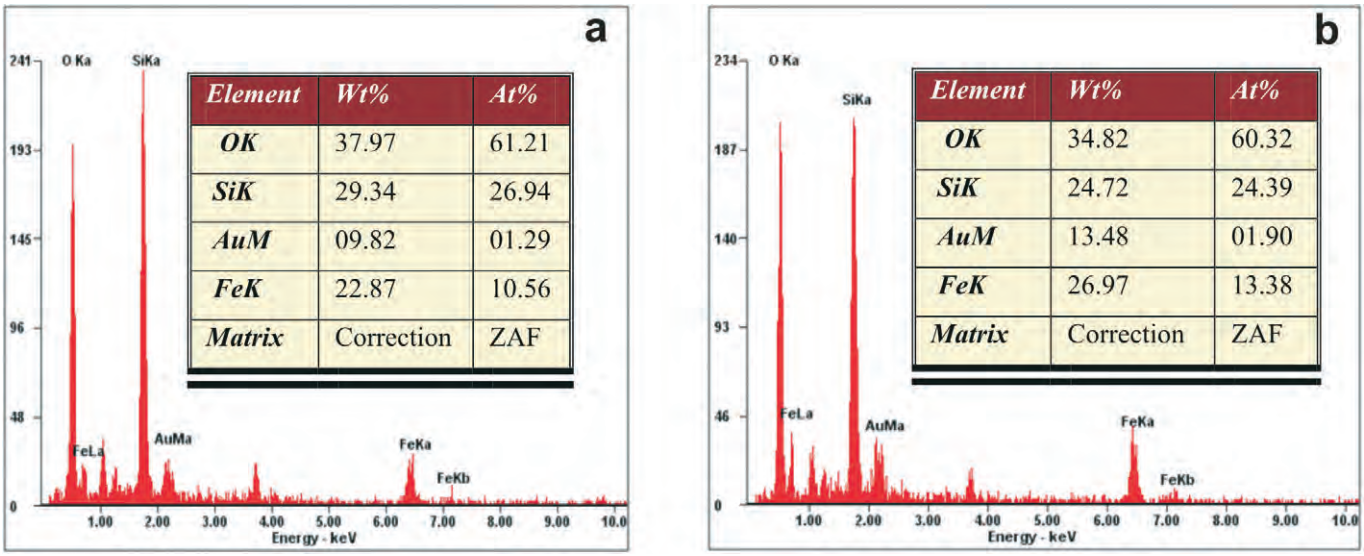


**Figure 2** EDAX plots of (**a**) FeOOH and (**b**) $mFe_3O_4$ nanoparticles.

(Fig. 2a,b) confirm the presence of iron (Fe). Moreover, the presence of oxygen (O), silicon (Si) and gold (Au) is also indicated in the plots. The presence of silicon and oxygen is due to the fact that the sample preparation was done over a thin glass film which is mainly composed of silicates (compound of Si and O). The high percentage of oxygen also indicates the formation of an oxide of iron. Furthermore, the presence of gold in the sample indicated in the EDAX plot arises from the gold polish that was used to prevent overcharging of the sample. From the EDAX plots obtained for FeOOH (Fig. 2a) and $Fe_3O_4$ (Fig. 2b) it is clear that the atom percentage of iron (Fe) is different for the two samples. Since the atomic ratio of Fe to O in FeOOH is 1:2 and that in $Fe_3O_4$ is 1.5:2, the atom percentage of Fe is more in case of $Fe_3O_4$ as compared with FeOOH which is clearly confirmed in the EDAX plots. This interpretation evidently confirms the formation of two different types of compounds. However, since EDAX is not generally considered as the best way to confirm the percentage of lighter elements like oxygen in any compound hence XRD analysis was performed to support the results. The histograms (Fig. 3a,b) obtained by visual FESEM image interpretation data indicate that the average diameter of FeOOH and $Fe_3O_4$ nanoparticles is of the order of 15–30 and 20–30 nm, respectively.

The XRD patterns of the synthesized FeOOH and $Fe_3O_4$

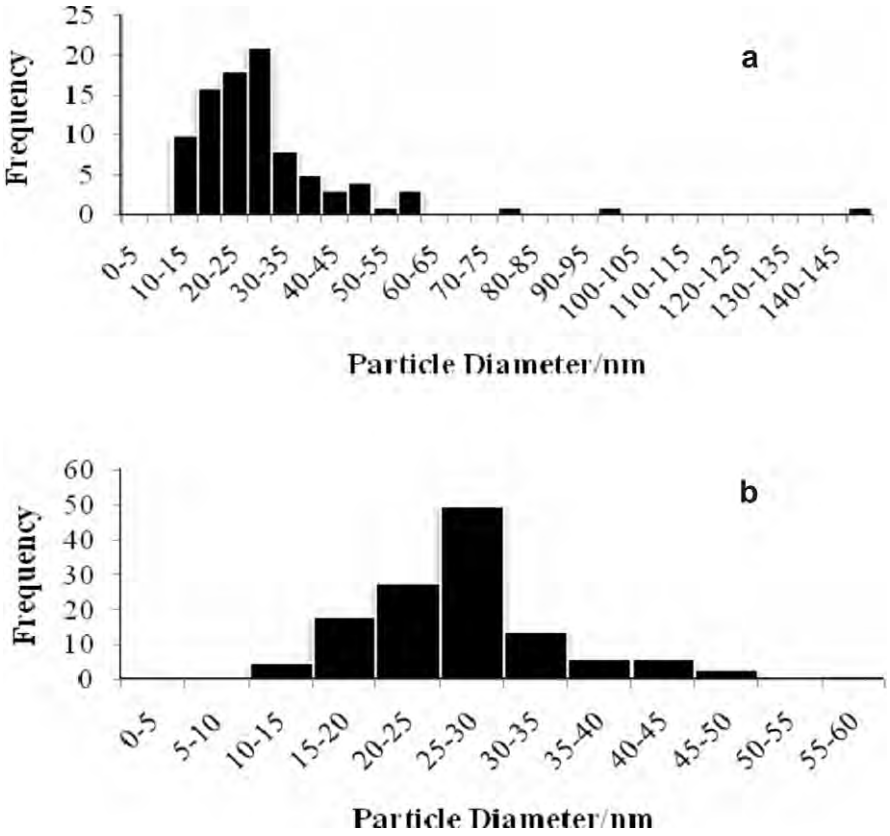


**Figure 3** Histograms of the particle diameter distributions for (**b**) FeOOH and (**b**) $Fe_3O_4$ nanoparticles.

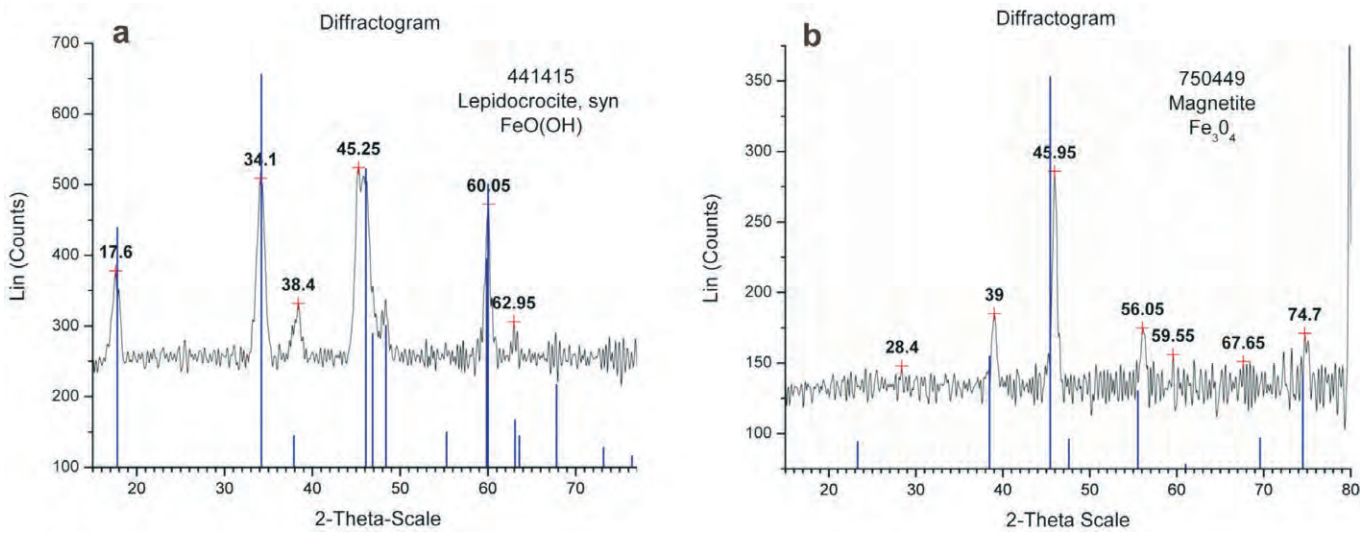


**Figure 4** Match between the diffractograms obtained for the (**a**) FeOOH and (**b**) $Fe_3O_4$ nanoparticles with those of the standard data base (shown in blue).

nanoparticles are shown in Fig. 4a and Fig. 4b, respectively. The diffractograms obtained from the XRD data analysis of FeOOH and $Fe_3O_4$ nanoparticles were matched with the standard database (JCPDS International Centre for Diffraction Data, 1998) by using PCPDFWIN Version 2.00 software. In both the diffractograms various peaks were found to match with the standard database. The blue coloured lines in Fig. 4a and Fig. 4b show the peak positions and intensities as per the existing JCPDS, 1998 database.

The diffractogram shown in Fig. 4a matches completely with that in the JCPDF database (number 441415) thereby confirming the formation of FeOOH (lepidocrocite, *syn*) nanoparticles. Similarly the match of the diffractogram shown in Fig. 4b with that in the JCPDF database (number 750449) confirms the formation of $Fe_3O_4$ (magnetite) nanoparticles. In this figure each peak position was found to be shifted by a constant 2-theta value of 5 degrees which may be due to some instrumental zero error. The matched database numbers 441415 and 750449, as determined from the PCPDFWIN Version 2.00 software for the compounds FeOOH and $Fe_3O_4$, suggests their crystal structures to be orthorhombic and cubic in nature, respectively.

The mean crystallite size and crystal plane spacing (d-value) as calculated for both types of nanoparticles are tabulated in Table 1a,b. The Miller indices and unit cell edge values for $Fe_3O_4$ and FeOOH nanoparticles are tabulated in Table 2a,b,c). From calculations the unit cell volume for $Fe_3O_4$ and FeOOH nanoparticles were found to be 126.41 Å$^3$ and 153.55 Å$^3$, respectively.

### 3.2. Degradation Studies of $CCl_4$

Both of the synthesized and properly characterized nanoparticles were employed for the degradation of $CCl_4$ in separate batches. Table 3a,b shows the chloride ion concentrations measured by means of an ion selective electrode at different time intervals for different $CCl_4$ starting concentrations employing FeOOH and $Fe_3O_4$ nanoparticles, respectively. From Fig. 5a and Fig. 5b it is clear that the chloride ion concentration increases with time. The chloride ion concentration shows higher values for higher concentrations of reactant $CCl_4$. An Increase in the chloride ion concentration is attributed to the increased degradation of $CCl_4$ which releases chloride ions into the solution.

The differential method was used to calculate the order of the reaction (n) and the rate constant (k). In order to determine the slope of the tangents for initial reaction time, the tangents were drawn to the curves in Fig. 5a and Fig. 5b at time t = 1.5 min. All the data points in Fig. 6a and Fig. 6b were found to lie on a straight line. The values of the slope n thus evaluated from

**Table 1** (**a**) Crystallite size obtained from Scherrer's formula for FeOOH nanoparticles.

| Peak No. | 2$\theta$/degree | d-value/Å | Baseline ($y_1$) /counts | Peak max. ($y_2$) /counts | $y_1 + \frac{(y_2 - y_1)}{2}$ | 2$\theta$ High /degree | 2$\theta$ Low /degree | FWHM /radians | Crystallite size/nm |
|---|---|---|---|---|---|---|---|---|---|
| 1 | 17.60 | 6.3275 | 250.0 | 378.0 | 314.0 | 18.1545 | 17.1400 | 0.01771 | 9.8437 |
| 2 | 34.10 | 3.3014 | 250.0 | 509.0 | 379.5 | 34.6882 | 33.5722 | 0.01948 | 9.2490 |
| 3 | 45.25 | 2.5163 | 250.0 | 524.0 | 387.0 | 46.6095 | 44.8300 | 0.03107 | 6.0078 |
| 4 | 60.05 | 1.9345 | 250.0 | 472.0 | 361.0 | 60.2362 | 59.6250 | 0.01067 | 18.6467 |

(**b**) Crystallite size obtained from Scherrer's formula for $Fe_3O_4$ nanoparticles.

| Peak No. | 2$\theta$/degree | d-value/Å | Baseline ($y_1$) /counts | Peak max. ($y_2$) /counts | $y_1 + \frac{(y_2 - y_1)}{2}$ | 2$\theta$ High /degree | 2$\theta$ Low /degree | FWHM /radians | Crystallite size/nm |
|---|---|---|---|---|---|---|---|---|---|
| 1 | 39.0 | 2.8999 | 136.0 | 185.0 | 160.5 | 39.2957 | 38.6719 | 0.0108 | 16.7827 |
| 2 | 46.0 | 2.4800 | 136.0 | 286.0 | 211.0 | 46.2583 | 45.6500 | 0.0106 | 17.6196 |
| 3 | 56.1 | 2.0602 | 136.0 | 175.0 | 155.5 | 56.4467 | 55.8541 | 0.0103 | 18.8630 |
| 4 | 74.7 | 1.5955 | 136.0 | 171.0 | 153.5 | 75.2391 | 74.5903 | 0.0113 | 19.1331 |

**Table 2** (**a**) Miller indices (h k l) for FeOOH nanoparticles.

| Peak No. | 2$\theta$/degree | d-value/Å | h k l |
|---|---|---|---|
| 1 | 17.60 | 6.3275 | 2 0 0 |
| 2 | 34.10 | 3.3015 | 2 1 0 |
| 3 | 45.25 | 2.5163 | 3 0 1 |
| 4 | 60.05 | 1.9345 | 0 2 0 |

(**b**) Unit cell edges and volume for FeOOH nanoparticles.

| Unit cell edges | | | Unit cell volume abc/Å$^3$ |
|---|---|---|---|
| a value/Å | b value/Å | c value/Å | |
| 12.6552 | 3.8701 | 3.1352 | 153.5517 |

(**c**) Miller indices (h k l) and unit cell edge values for $Fe_3O_4$ nanoparticles.

| Peak No. | 2$\theta$/degree | Sin$^2\theta$ | 1*(Sin$^2\theta$/Sin$^2\theta_{min}$) | 2*(Sin$^2\theta$/Sin$^2\theta_{min}$) | 3*(Sin$^2\theta$/Sin$^2\theta_{min}$) | $h^2+k^2+l^2$ | h k l | d-value/Å | Unit cell edge 'a' value/Å |
|---|---|---|---|---|---|---|---|---|---|
| 1 | 39.0 | 0.11142 | 1.000000 | 2.000000 | 3.000000 | 3 | 111 | 2.8999 | 5.0228 |
| 2 | 46.0 | 0.15267 | 1.370144 | 2.740288 | 4.110432 | 4 | 200 | 2.4800 | 4.9600 |
| 3 | 56.1 | 0.22112 | 1.984501 | 3.969002 | 5.953503 | 6 | 211 | 2.0602 | 5.0465 |
| 4 | 74.7 | 0.36806 | 3.303176 | 6.606352 | 9.909528 | 10 | 310 | 1.5956 | 5.0457 |

**Table 3** (**a**) Variation of the chloride ion concentration with time for different initial $CCl_4$ concentrations obtained with FeOOH nanoparticles.

| Initial $CCl_4$ conc. 250 ppm | | Initial $CCl_4$ conc. 500 ppm | | Initial $CCl_4$ conc. 750 ppm | | Initial $CCl_4$ conc. 1000 ppm | |
|---|---|---|---|---|---|---|---|
| Time/min | $[Cl]^-$/ppm | Time/min | $[Cl]^-$/ppm | Time/min | $[Cl]^-$/ppm | Time/min | $[Cl]^-$/ppm |
| 0 | 0 | 0 | 0 | 0 | 0 | 0 | 0 |
| 4 | 0.13 | 5 | 0.38 | 5 | 0.83 | 4 | 1.54 |
| 8 | 0.24 | 8 | 0.58 | 8 | 1.15 | 9 | 2.88 |
| 14 | 0.52 | 13 | 1.05 | 13 | 1.98 | 14 | 4.27 |
| 19 | 0.65 | 19 | 1.28 | 19 | 2.77 | 20 | 6.57 |
| 23 | 0.89 | 22 | 1.53 | 22 | 3.53 | 25 | 7.67 |
| 29 | 1.06 | 27 | 1.74 | 27 | 3.91 | 30 | 8.87 |
| 33 | 1.28 | 32 | 2.09 | 32 | 4.38 | | |
| 40 | 1.66 | 39 | 2.68 | 39 | 5.23 | | |
| 45 | 1.75 | 45 | 3.05 | 45 | 5.99 | | |
| 51 | 1.85 | | | | | | |

(**b**) Variation of the chloride ion concentration with time for different initial $CCl_4$ concentrations obtained with $Fe_3O_4$ nanoparticles.

| Initial $CCl_4$ conc. 250 ppm | | Initial $CCl_4$ conc. 500 ppm | | Initial $CCl_4$ conc. 750 ppm | | Initial $CCl_4$ conc. 1000 ppm | |
|---|---|---|---|---|---|---|---|
| Time/min | $[Cl]^-$/ppm | Time/min | $[Cl]^-$/ppm | Time/min | $[Cl]^-$/ppm | Time/min | $[Cl]^-$/ppm |
| 0 | 0 | 0 | 0 | 0 | 0 | 0 | 0 |
| 6 | 10 | 6 | 17 | 5 | 32 | 6 | 45 |
| 12 | 19 | 13 | 29 | 12 | 59 | 10 | 63 |
| 16 | 25 | 17 | 46 | 16 | 72 | 15 | 76 |
| 20 | 31 | 24 | 57 | 19 | 78 | 19 | 89 |
| 26 | 40 | 29 | 66 | 25 | 94 | 26 | 106 |
| 31 | 52 | 36 | 78 | 32 | 105 | 32 | 116 |
| 35 | 53 | | | 37 | 108 | | |
| 40 | 57 | | | | | | |

Fig. 6a and Fig. 6b were found to be 1.7739 and 1.3042, respectively, which are nearly equal to 2 and 1. This confirms the reactions to be second-order for FeOOH and first-order for $Fe_3O_4$. Moreover, the value of the rate constant k is $1.4 \times 10^{-6}$ ppm$^{-1}$ min$^{-1}$ for FeOOH and $9.58 \times 10^{-4}$ min$^{-1}$ for $Fe_3O_4$.

## 4. Conclusions

Batch degradation studies of $CCl_4$ employing both types of nanoparticles suggest that the reactivity of freshly synthesized $Fe_3O_4$ nanoparticles is much higher compared to that of freshly synthesized FeOOH nanoparticles. For example, the concentration of the product chloride ion obtained from the degradation of 60 ppm of $CCl_4$ with FeOOH nanoparticles in 30 min was only 8.87 ppm while that degraded by the same amount of $Fe_3O_4$ nanoparticles was about 112 ppm. The concentration of chloride ion obtained is proportional to the amount of $CCl_4$ degraded hence the greater the degradation of $CCl_4$, the greater will be the chloride ion concentration. Similar results were obtained for all

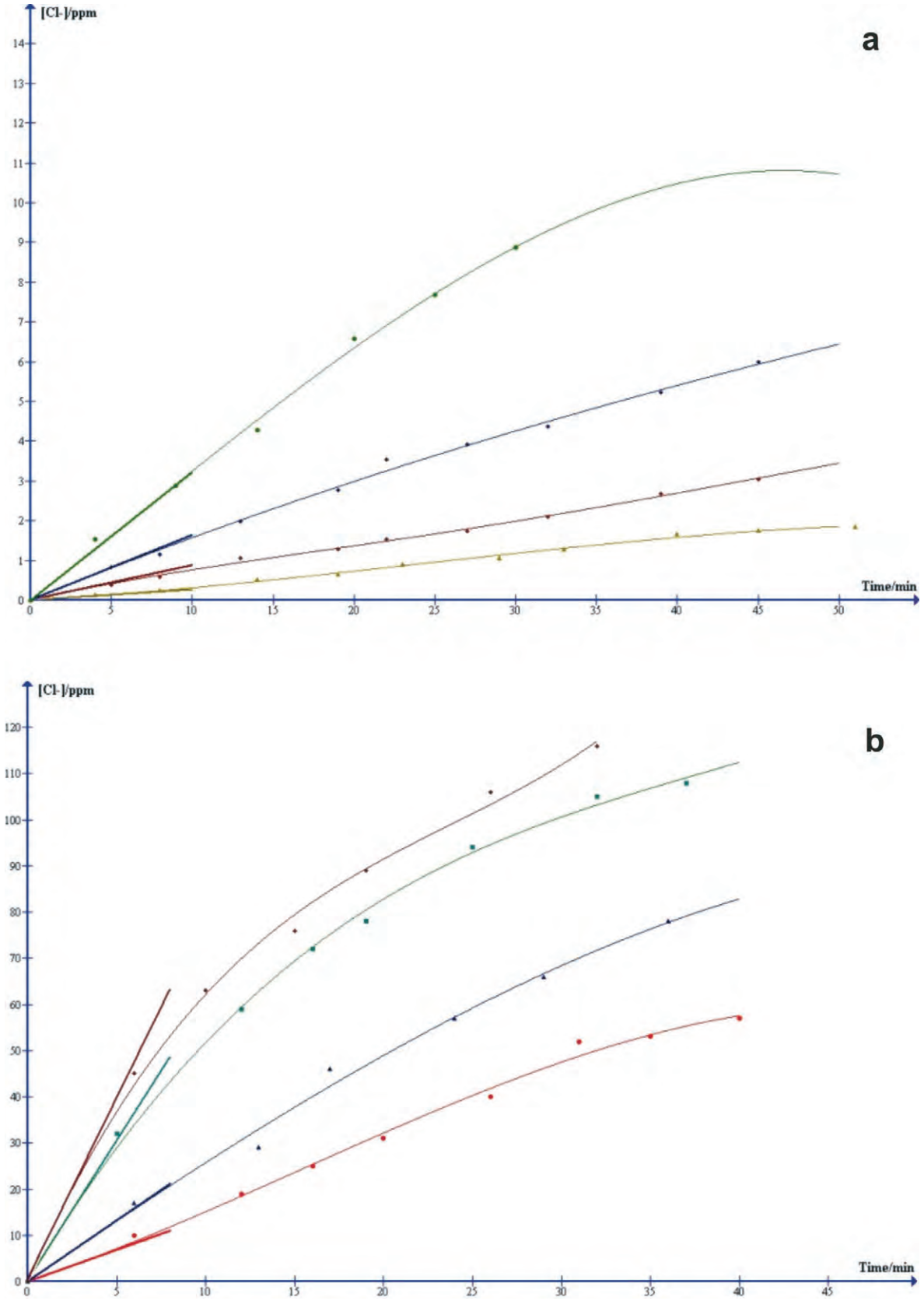


**Figure 5** (**a**) Increase in the chloride ion concentration with time for the degradation of $CCl_4$ with FeOOH nanoparticles. (**b**) Increase in the chloride ion concentration with time for the degradation of $CCl_4$ with $Fe_3O_4$ nanoparticles.

the four concentrations of $CCl_4$ tested. The degradation of $CCl_4$ with freshly synthesized $Fe_3O_4$ and FeOOH nanoparticles follows first- and second-order kinetics, respectively. Further, it can be concluded that the decreased reactivity of FeOOH nanoparticles may be due to the changed oxidation of the Fe centre in FeOOH.

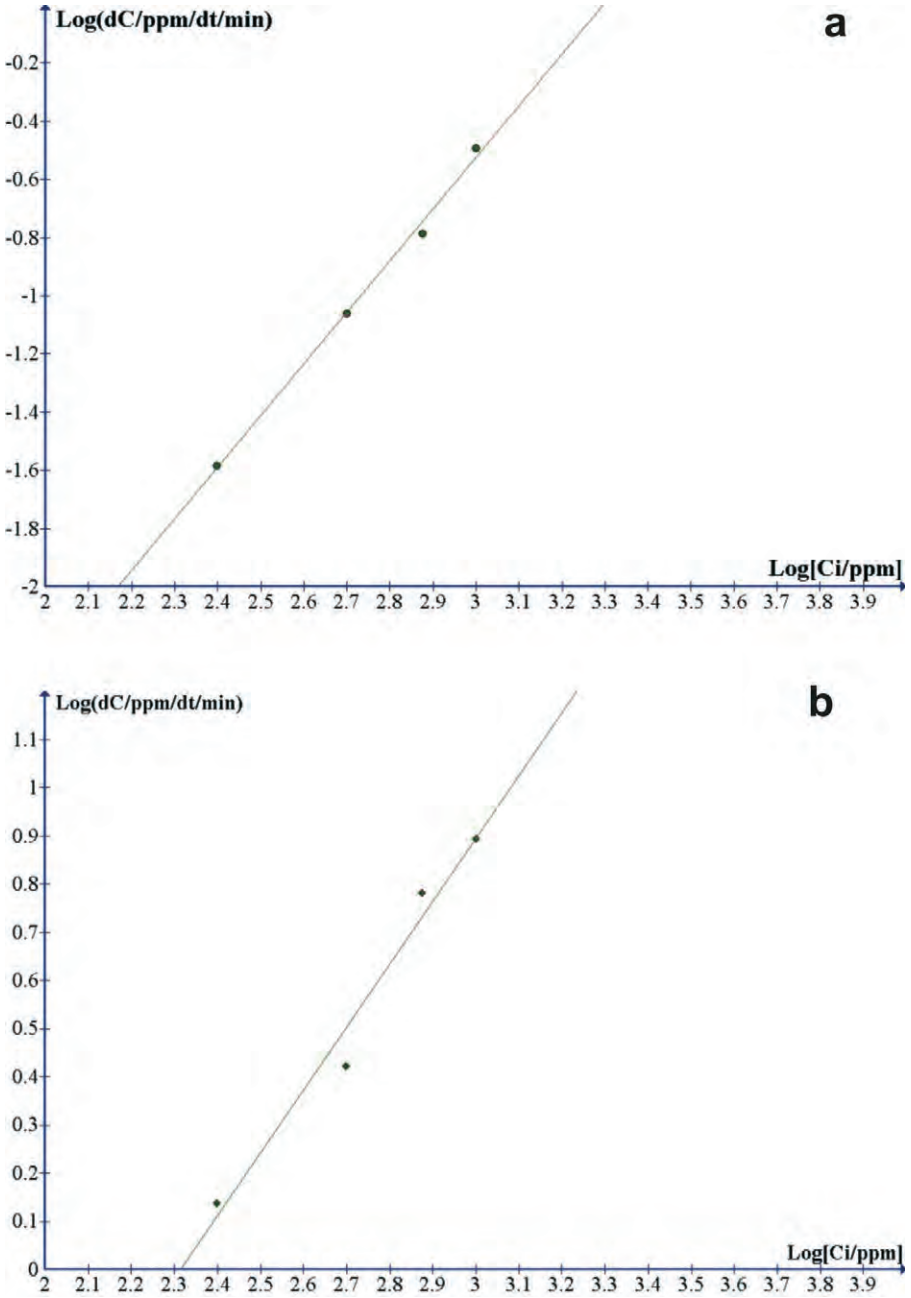


**Figure 6** (**a**) Plot to determine the order of reaction and rate constant for the degradation of $CCl_4$ with FeOOH nanoparticles. (**b**) Plot to determine the order of reaction and rate constant for the degradation of $CCl_4$ with $Fe_3O_4$ nanoparticles.

## ACKNOWLEDGEMENTS

Many thanks go to the Council for Scientific and Industrial Research (CSIR), New Delhi, India, for the award of Junior Research Fellowship to Ashutosh Agarwal. Thanks are also due to the Head, Institute Instrumentation Centre, IIT Roorkee, for the use of the FESEM and XRD facilities.

## REFERENCES

1 C.J. Tsai, M.L. Chen, K.F. Chang, F.K. Chang and I.F. Mao, *Chemosphere,* 2009, **74**, 1104–1110.
2 W.A. Arnold and A.L. Roberts, *Environ. Sci. Technol.,* 1998, **32**, 3017–3025.
3 W.A. Arnold and A.L. Roberts, *Environ. Sci. Technol.,* 2000, **34**, 1794–1805.
4 S. Choe, S.H. Lee, Y.Y. Chang, K.Y. Hwang and J. Khim, *Chemosphere,* 200, **42**, 367–372.
5 C.J. Clark II, P.S.C. Rao and M.D. Annable, *J. Hazard. Mater.,* 2003, **96**, 65–78.
6 T.L. Johnson, M.M. Scherer and P.G. Tratnyek, *Environ. Sci. Technol.,* 1996, **30**, 2634–2640.
7 L.J. Matheson and P.G. Tratnyek, *Environ. Sci. Technol.,* 1994, **28**, 2045–2053.
8 J. Morales, R. Hutcheson and I.F. Cheng, *J. Hazard. Mater.,* 2002, **90**, 97–108.
9 A.L. Roberts, L.A. Totten, W.A. Arnold, D.R. Burris and T.J. Campbell, *Environ. Sci. Technol.,* 1996, **30**, 2654–2659.
10 C.G. Schreier and M. Reinhard, *Chemosphere,* 1994, **29**, 1743–1753.
11 B. Schrick, S.M. Ponder and T.E. Mallouk, ACS National Meeting Book of Abstracts, 2000, **40**, 639–640.
12 C.B. Wang and W.X. Zhang, *Environ. Sci. Technol.,* 1997, **31**, 2154–2156.
13 W.X. Zhang, C.B. Wang and H.L. Lien, *Catalysis Today,* 1998, **40**, 387–395.
14 A. Agarwal, H. Joshi and A. Kumar, *Recent Research in Sci. Technol.,* 2011, **3**(1), 5–15
15 B.D. Cullity, *Elements of X-ray Diffraction*, Addison-Wesley Publishing Company, Massachusetts, 1978.